# Ank3-dependent SVZ niche assembly is required for the continued production of new neurons

**Patricia Paez-Gonzalez**[1,2], **Khadar Abdi**[1,2], **Dominic Luciano**[3], **Yan Liu**[1], **Mario Soriano-Navarro**[4], **Emma Rawlins**[1,5], **Vann Bennett**[1,6], **Jose Garcia-Verdugo**[4], and **Chay T. Kuo**[1,2,3,7,8,*]

[1]Department of Cell Biology, Duke University Medical Center, Durham, NC 27710, USA

[2]Brumley Neonatal-Perinatal Research Institute, Department of Pediatrics, Duke University Medical Center, Durham, NC 27710, USA

[3]Department of Neurobiology, Duke University Medical Center, Durham, NC 27710, USA

[4]Laboratorio de Morfología Celular, Unidad mixta CIPF-UVEG, CIBERNED. Valencia, Spain

[6]Howard Hughes Medical Institute, Duke University Medical Center, Durham, NC 27710, USA

[7]Preston Robert Tisch Brain Tumor Center, Duke University Medical Center, Durham, NC 27710, USA

[8]Duke University Institute for Brain Sciences, Durham, NC 27708, USA

## SUMMARY

The rodent subventricular/subependymal zone (SVZ/SEZ) houses neural stem cells (NSCs) that generate olfactory bulb interneurons. It is unclear how the SVZ environment sustains neuronal production into adulthood. We discovered that the adapter molecule Ankyrin-3 (Ank3) is specifically upregulated in radial glia destined to become SVZ ependymal niche cells, but not in NSCs, and is required for SVZ assembly through progenitor lateral adhesion. Furthermore, we found that Ank3 expression is controlled by Foxj1, a transcriptional regulator of multicilia formation, and genetic deletion of this pathway led to complete loss of SVZ niche structure. In its absence, radial glia continued to transition into postnatal NSCs. However, inducible ependymal deletion of Foxj1-Ank3 after SVZ niche assembly resulted in dramatic depletion of neurogenesis. Targeting a novel pathway regulating ependymal organization/assembly and showing its requirement for new neuron production, our results have important implications for environmental control of adult neurogenesis and harvesting NSCs for replacement therapy.

*Corresponding author: chay.kuo@duke.edu .
[5]Present address: The Gurdon Institute, University of Cambridge, CB2 1QN, UK

**SUPPLEMENTAL INFORMATION**

Supplemental information for this article includes one table, eight figures, five movies, experimental procedures and associated references, and can be found with this article online.

## INTRODUCTION

Throughout embryonic and postnatal development, neural progenitors / stem cells give rise to differentiated neurons, astrocytes, and oligodendrocytes (Gotz and Huttner, 2005; Kokovay et al., 2008; Kriegstein and Alvarez-Buylla, 2009). While these progenitors are relatively abundant during embryogenesis, they become restricted to specialized regions / niches in the adult brain including the subventricular/subependymal zone (SVZ/SEZ) along the lateral walls of lateral brain ventricles, as well as the subgranular zone in the dentate gyrus of the hippocampus (Miller and Gauthier-Fisher, 2009; Suh et al., 2009). Adult neurogenesis in the rodent SVZ is mediated by type B astrocytes functioning as neural stem cells (NSCs) (Doetsch et al., 1999), which in turn differentiate into neuroblasts that migrate and incorporate into the mouse olfactory bulb as interneurons (Lledo et al., 2008). This source of new neurons provides a key experimental system for studying neuronal integration into functional circuits (Kelsch et al., 2010), as well as holding promising therapeutic potential. However, the exact mechanisms allowing for continuation of neurogenesis into adulthood in this brain region are not well understood.

NSCs in the adult SVZ exist in a dedicated environment that is comprised mainly of multiciliated ependymal cells on the ventricular surface, as well as a specialized vascular network (Alvarez-Buylla and Lim, 2004). Arrangement of this "niche" is spatially defined, in that ependymal cells are organized in a pinwheel-like fashion surrounding monociliated NSCs touching the ventricular surface (Mirzadeh et al., 2008). In addition, SVZ NSCs extend basal processes that terminate on blood vessels that lie beneath the ependymal layer (Shen et al., 2008; Tavazoie et al., 2008). The SVZ niche is a rich source for growth factors and specialized cell-cell interactions that maintain NSC homeostasis in vivo (Miller and Gauthier-Fisher, 2009; Kokovay et al., 2010), and it can respond to environmental challenges by modifying the proliferative/differentiation capacities of NSCs (Kuo et al., 2006; Luo et al., 2008; Carlen et al., 2009). Despite this knowledge, there is no direct evidence that this defined SVZ architecture is required for the continued production of new neurons - due largely to our inability to specifically eliminate the SVZ niche. We previously generated one of the first inducible mouse models to postnatally disrupt SVZ architecture via Numb/Numblike deletion, revealing a local remodeling capacity (Kuo et al., 2006), however, the ensuing ventriculomegaly precluded functional assessment on adult neurogenesis, as the flow of cerebrospinal fluid has been shown to regulate migration of newborn neurons (Sawamoto et al., 2006). These results point to the importance of identifying SVZ niche-specific pathways to allow for direct deletion of SVZ architecture without cell-intrinsically affecting NSCs.

Little is known about the molecular mechanisms controlling SVZ generation from embryonic progenitors. Shortly before and after birth, while most embryonic radial glia terminally differentiate, postnatal radial glial progenitors (pRGPs) along the lateral walls of lateral ventricles generate the SVZ niche (Tramontin et al., 2003). The transformation from embryonic to adult neurogenesis is mediated by a subpopulation of pRGPs differentiating into SVZ NSCs (Merkle et al., 2004). A second subpopulation of pRGPs gives rise to ependymal cells that form the new epithelial lining of the brain ventricles, which also serve as multiciliated niche cells for the SVZ NSCs (Spassky et al., 2005). We showed previously that during terminal differentiation of pRGPs, progenitors begin to modify their lateral membrane contacts (Kuo et al., 2006). The Ankyrin family of proteins in mammals, consisting of Ankyrin R (1, Ank1), B (2, Ank2), and G (3, Ank3), are large adapter molecules that organize membrane domains in a number of different cell types, including erythrocytes, cardiac and skeletal muscles, epithelial cells, retinal photoreceptors, and neuronal axon initial segments (Bennett and Healy, 2008). Although Ankyrins and their homologues in other model organisms have not been linked to stem cell niche functions,

Ank3 is known to regulate lateral membrane biogenesis of bronchial epithelial cells, through collaborative interactions with β2-Spectrin and α-Adducin (Kizhatil and Bennett, 2004; Abdi and Bennett, 2008).

Using in vivo inducible genetics and newly developed in vitro assays, we revealed a novel function for Ank3 and its upstream regulator in radial glial assembly of adult SVZ niche, which upon disruption led to the complete absence of SVZ ependymal niche in vivo. The revelation of these key early molecular steps allowed us to address fundamental questions about SVZ organization on continued production of new neurons.

## RESULTS

### Selective Ank3 upregulation in subpopulation of pRGPs during SVZ formation

Since the SVZ niche is formed during postnatal maturation of the brain ventricular wall, we performed surface scanning electron microscopy (SEM) and transmission electron microscopy (TEM) on mouse brains from postnatal days 0, 7, and 14 to observe anatomical changes (P0, P7, P14, Figure S1A). Unlike the medial wall surface, which showed abundant multiciliated cells throughout, at P0 the cells on the lateral wall were predominantly monociliated and gradually became multiciliated over the next 2 weeks. Concurrently, there was considerable specialization of cellular lateral membranes, as pRGP contacts transitioned from simple apical adherens junctions at P0, to mature interdigitating membranes between ependymal cells with mixtures of adherens and tight junctions by P14 (Figure S1B). These developmental processes take place during the critical period when the SVZ neurogenic niche is assembled from pRGPs.

We wondered if specialization of progenitor lateral membranes is required for SVZ niche assembly. Within the Ankyrin family of proteins, Ank1 is largely erythroid-specific, therefore we looked for Ank2 and Ank3 expressions within the SVZ niche. Immunohistochemical (IHC) staining with Ank2- and Ank3-specific antibodies on P14 brain lateral ventricular wholemounts demonstrated that while Ank2 was ubiquitously expressed, Ank3 was specifically localized to the lateral cellular borders of multiciliated ependymal cells, but not to the monociliated cells at the center of pinwheel-like niche structures containing NSCs (Figure 1A).

To understand the selectivity of this Ank3 expression during postnatal SVZ formation, we performed IHC staining on ventricular wall wholemounts at different postnatal stages from Foxj1-GFP mice (Ostrowski et al., 2003). The Foxj1-GFP reporter line has been shown to efficiently label ependymal cells and their progenitors (Zhang et al., 2007; Jacquet et al., 2009). At P0, all Ank3$^+$ cells co-localized with GFP, although some GFP-dim cells were Ank3$^-$ (Figure 1B). However, by P14 Ank3 showed specific co-localization with Foxj1-GFP labeling, and the protein became highly concentrated at the lateral cellular borders (Figure 1B). We next imaged in the x-z plane and confirmed that as Foxj1-GFP$^+$ pRGPs transitioned from radial glia to fully-differentiated ependymal cells, Ank3 became enriched at lateral cellular borders (Figure 1C). Since Ank3 is expressed by mature neurons and enriched in the axon initial segment, as expected on coronal sections from P14 brains we saw high level expression in striatal neurons (Figure 1D). However, within the SVZ, just beneath the S100β$^+$Ank3$^+$ ependymal layer, we did not detect Ank3 expression (Figure 1D, asterisks). Co-staining with GFAP and DCX antibodies showed that both SVZ astrocytes and newborn neuroblasts within the SVZ were Ank3 negative (Figure 1D and S1C). These results revealed Ank3 as one of the first molecules identified that is differentially expressed on the lateral membranes between SVZ NSCs and ependymal niche cells.

## Self-organization of pRGPs into ependymal clusters

Due to the complexity of the *ank3* genomic locus (the 190 kD splice-form alone has 43 exons spanning roughly 500 kb of genomic sequence), previous attempts to generate *ank3*-deficient mice have only resulted in splice-form specific deletions in cerebellar neurons (Zhou et al., 1998). To determine the function for Ank3 during SVZ neurogenesis, we set out to develop a primary cell culture assay to generate SVZ ependymal niche cells. Using a modified protocol based on existing methods (Prothmann et al., 2001; Guirao et al., 2010), we were able to differentiate pRGPs from P0 mice into large numbers of multiciliated ependymal cells with beating cilia (Movie S1). IHC staining against γ-Tubulin showed the transition from single to multiple basal bodies in multiciliated cells after differentiation (Figure 2A). These pRGPs also progressed from Glast$^{hi}$/S100β$^{lo}$ to Glast$^{lo}$/S100β$^{hi}$ during differentiation (Figure 2A), consistent with our previous observation for postnatal ependymal differentiation in vivo (Kuo et al., 2006). Quantifying γ-Tubulin cluster staining as a percentage of DAPI nuclear staining, 64±6.5% s.d. of total cells after completion of differentiation became multiciliated.

We noticed that differentiated ependymal cells often clustered in culture, and SEM analyses showed multiciliated cells arranged in clusters around monociliated cells (Figures 2B and S2A), much like their in vivo organization (Mirzadeh et al., 2008). The monociliated cells within ependymal clusters were also GFAP$^+$ in culture (Figures 2C and S2B). To understand the processes leading to pRGP clustering in vitro, we performed live cell imaging using the Foxj1-GFP reporter mouse line (Ostrowski et al., 2003). We observed that shortly after plating, there was an increase in the number of GFP$^+$ pRGPs, followed by upregulation of GFP expression and cellular clustering (Movie S2). Expansion in the number of GFP$^+$ cells was accomplished by both progenitors starting to express GFP as well as by cell division (Movie S3). It is interesting to note that the majority of GFP$^+$ pRGP clustering took place 3 to 4 days after plating, prior to the appearance of multicilia, which began 7 to 8 days after plating (Movie S2 and Figure 2D). Once the clustering was complete, these structures were positionally stable (Movie S2). IHC staining revealed that the clusters represented multiciliated Foxj1-GFP$^+$ arranged around monociliated GFP$^-$ cells (Figure S2C).

## Ank3 is required for proper SVZ niche assembly

To understand if this pRGP culture may be useful for tackling Ank3 function, we saw that during in vitro differentiation, pRGP clusters upregulated Ank3 along their cell borders, prior to multicilia formation (Figure 3A). Western blot analyses of pRGP cultures confirmed robust increase in the 190 kD Ank3 protein (known to be an epithelial-specific splice-form) (Kizhatil et al., 2007) after differentiation, as well as Ank3-associated proteins β2-spectrin and α-Adducin (Figure 3B). We wanted to know whether Ank3 expression/localization is dependent on multicilia formation in SVZ ependymal cells. Using a tamoxifen-inducible *foxj1-CreER$^{t2}$* transgene (Rawlins et al., 2007), we deleted Kif3a, a critical molecular motor for cilia formation (Marszalek et al., 2000), from postnatal pRGPs. Lineage tracing analyses of the *foxj1-creER$^{t2}$; rosa26-YFP* reporter mice injected with tamoxifen at birth and analyzed at P14 showed that Foxj1-CreER$^{t2}$ can target multiciliated ependymal cells (Figure S3A). We generated clonal deletion of Kif3a in pRGPs by low-dose tamoxifen injection into newborn *foxj1-creER$^{t2}$; kif3a$^{KO/Flox}$* mice. When analyzed at P14, Kif3a mutant ependymal patches, lacking surface acetylated-tubulin staining for multicilia, were able to properly express and localize Ank3 to their lateral borders (Figure S3B).

We then generated lentiviral construct expressing shRNA against mouse Ank3, and tested this in NIH 3T3 cells, which knocked-down greater than 95% of endogenous Ank3 after lentiviral infection (Figure S4A). We next made lentivirus co-expressing this shRNA and GFP under control of the 1-kb human Foxj1 promoter (the same promoter used to generate

the Foxj1-GFP transgene) (Ostrowski et al., 2003), and infected pRGP cultures 24 hours after plating. Lentiviral infection of pRGPs was highly efficient as more than 90% of multiciliated cells (assessed by γ-Tubulin/DAPI staining) became GFP[+] after differentiation (Figure 3C and data not shown). While control virus-infected pRGPs upregulated Ank3 in clusters as normal, we were able to knockdown this expression with the Ank3 shRNA virus (Figure 3C).

As GFP expression in infected cells did not become bright enough for live imaging until 3-4 days after infection (too late for following cellular clustering in real time), we used antibody staining to quantify the ability of infected pRGPs to cluster after differentiation (Figure S4B). Counting cells stained with GFAP, γ-Tubulin, and Phalloidin, we found that Ank3 shRNA-infected pRGPs had significantly reduced numbers of clustered structures when compared to control virus-infected cultures (Figure 3D). To confirm these findings in vivo, we performed stereotactic injection of control and Ank3 shRNA lentiviruses into P0 mice, specifically targeting pRGPs through striatal injections (Merkle et al., 2004). Ventricular wholemount staining 5 days after lentiviral injection showed that control pRGPs were able to assemble into clustered structures, with Ank3^{+} ependymal cells exhibiting large apical surface areas surrounding Ank3^{−} cells with small apical surfaces (Figure S4C). In contrast, Ank3 knocked-down pRGPs failed to organize into clusters along the ventricular surface, and retained a smaller apical surface area (by Phalloidin staining) as compared to neighboring cells with intact Ank3 expression (Figure S4C). Furthermore, whereas the Ank3^{+} pRGPs had largely down-regulated immature ependymal marker Glast (Figure 3E), Ank3 knocked-down pRGPs retained high-level Glast expression, showed disorganized patterning, and failed to differentiate into mature multiciliated ependymal cells (Figure 3E).

## Absence of postnatal Ank3 upregulation in conditional Foxj1-mutant pRGPs

Since striatal lentiviral injection can only target a small number of pRGPs, we would like to remove Ank3 function in vivo. One strategy is to delete its upstream regulator in pRGPs to prevent Ank3 expression. Transcriptional regulation of *ank3* (or any of the other Ankyrins) is not known. One candidate for such control, since its expression appears before Ank3 in pRGPs (Figure 1), is the transcription factor Foxj1. It is a well-established regulator of motile-cilia formation (Yu et al., 2008), as well as multicilia formation in ependymal cells (Brody et al., 2000; Jacquet et al., 2009). Due to severe defects in multiple organ systems, including the lung, most *foxj1*-null mice die within 3 days after birth (Brody et al., 2000). Despite a previous report (Jacquet et al., 2009), we did not obtain any null mutants surviving past P7 in more than 10 litters from crosses using the same *foxj1*-heterozygous mice (Brody et al., 2000).

To address nervous system-specific questions, we generated a conditional floxed allele of the *foxj1* gene (Brody et al., 2000) (Figure 4A). We crossed our *foxj1-flox* (*foxj1^{Flox/+}*) line to germ-line *β-actin-cre* mice to generate a knockout allele (*foxj1-KO*). We then crossed this *foxj1-KO* (*foxj1^{KO/+}*) allele to a *nestin-cre* driver (Tronche et al., 1999) and *foxj1^{Flox/Flox}* mice, and compared phenotypes between *nestin-cre; foxj1^{KO/Flox}* (cKO) and *nestin-cre; foxj1^{+/Flox}* (control) littermates. At birth, we could not detect histological differences in brain sections between control and cKO littermates, and lateral ventricle size in P3 cKO mice was comparable to controls (Figure S5A and data not shown). The cKO mice lived without obvious signs of defect until after P7, when hydrocephalus appeared from the lack of multicilia on maturing ependymal cells (Figure S5B). Staining of P5 cKO brain sections confirmed the removal of Foxj1 protein, normally expressed by the ependymal layer in control animals (Figure S5C).

IHC staining on brain ventricular wall wholemounts from P3 control and cKO mice showed that while Ank2 was normally expressed, Ank3 expression was absent from the developing

SVZ niche in cKO mice (Figure 4B). This loss was confirmed by Western blot analyses of differentiated pRGPs, also showing concurrent reduced levels for β2-Spectrin and α-Adducin (Figure 4C). IHC staining on ventricular wall wholemounts from P6 mice with antibodies against S100β and Glast showed that while pRGPs from control mice had matured into S100β$^{hi}$/Glast$^{lo}$ ependymal cells, those from mutant mice remained largely S100β$^{lo}$/Glast$^{hi}$, resembling immature pRGPs (Figure 4D). To determine if this phenotype was due to a failure of ependymal differentiation, or the generation of additional Glast$^+$ progenitors, we introduced by breeding the Foxj1-GFP transgenic reporter allele into the cKO background to visualize the fate of GFP$^+$ pRGPs. The possibility that Foxj1 auto-regulates the 1-kb human Foxj1 promoter in the Foxj1-GFP transgene appeared low since sequence analyses showed no predicted Foxj1 binding sites (Lim et al., 1997; Badis et al., 2009) within this promoter region (data not shown). In cKO mutant mice at P6, we detected robust Foxj1-GFP expression along the lateral ventricular surface, but these GFP$^+$ cells continued to express Glast with little to no S100β expression (Figure 4E). These results showed that in cKO mice, the ventricular wall is populated by Foxj1-GFP$^+$ progenitors destined to become SVZ niche cells, but failed to fully differentiate into S100β$^+$ ependymal cells.

## Ank3-mediated lateral membrane specialization defects in Foxj1-mutant pRGPs

Since Ankyrins mediate many aspects of membrane protein positioning, it is likely that several lateral membrane proteins and their molecular partners may be defective in cKO pRGPs lacking Ank3 (β2-Spectrin and α-Adducin for example, Figure 4C). TEM analyses showed that while ependymal progenitors in P4 control mice continued to mature their lateral membranes (compared to Figure S1B), in cKO mice both membrane interdigitation and adherens junctions were reduced (Figure 5A and S6A). Ank3 binds to E- and N-cadherin, and in epithelial cells is known to limit membrane diffusion of E-Cadherin in the lateral cell borders (Kizhatil et al., 2007). We found that N-cadherin protein level was greatly upregulated during in vitro pRGPs differentiation (Figure 5B), suggesting that a function for Ank3 upregulation in Foxj1$^+$ pRGPs could be to anchor newly synthesized N-cadherin at cell membranes. cKO pRGPs upregulated N-cadherin expression postnatally, and showed only mild reduction in protein level after in vitro differentiation compared to controls (Figure 5B and data not shown). Unsurprisingly, while ventricular wholemount staining from P4 control mice showed lateral organization of N-cadherin in many pRGPs during ongoing niche formation, this organization was difficult to detect in cKO littermates (Figure 5C).

To see if Ank3 can rescue this N-cadherin localization defect in Foxj1 mutant pRGPs, we generated lentiviral construct expressing the 190 kD splice-form of Ank3. In control pRGPs after in vitro differentiation, N-cadherin was co-localized with Ank3 to the lateral membranes (Figure 5D). However, in differentiated Foxj1 cKO pRGPs, N-cadherin became diffusely distributed throughout the cytoplasm (Figure 5D and S6B). Lentiviral expression of Ank3 allowed previously cytoplasmic N-cadherin to locate to the lateral borders in Foxj1 cKO pRGPs (Figures 5D and 5E). The reintroduced Ank3 protein in mutant pRGPs was less evenly distributed at the lateral membranes (Figure 5D), reflecting perhaps the heterogeneous nature of lentiviral-mediated Ank3 expression in these cells, as well as the possibility that additional molecules regulated by Foxj1 may work together with Ank3 to specialize progenitor lateral membranes.

To determine if Foxj1 can directly activate Ank3 expression in pRGPs, we first infected Foxj1 cKO pRGPs with a lentiviral construct expressing Foxj1 with a C-terminal Myc-tag. Both Western blots and IHC staining showed that Foxj1-Myc virus-infected cKO pRGPs were able to upregulate Ank3 protein expression (Figure 5F). Looking for direct Foxj1 binding sites within 1.4 million base-pairs (bps) of genomic sequence surrounding the *ank3*

locus (mm9.chr10:68,740,000-70,150,000), we searched for consensus DNA binding motifs based on published data (Lim et al., 1997; Badis et al., 2009) (Figure S6C). Using position frequency matrix on the predicted $^A/_G$TAAACA binding motif for Foxj1 (Bejerano et al., 2005), we identified 790 positions in this region that had a 90% or better sequence match (data not shown). Filtering by evolutionary conservation to orthologous positions in at least 20 other species (Karolchik et al., 2007), we narrowed this list down to 29 potential binding sites (Table S1). Looking for clustering of at least 2 sites close by, we identified a 500 bp region roughly 200 kb upstream of the 1st exon that contained 4 putative Foxj1 binding sites conserved in 21, 26, 31, and 25 species, respectively (5′ Enh, Figure S6C). We also identified 2 putative binding sites spaced 540 bps apart in the 3′ UTR of *ank3* that were conserved in 29 and 32 species (3′ Enh, Figure S6C).

Using purified GST-Foxj1 DNA binding domain fusion protein (Lim et al., 1997), we showed via oligonucleotide gel-shift assay that there was specific Foxj1 binding to each of these predicted elements, which can be disrupted by mutating the "T" and "C" positions in the binding motifs to "A"s (Figure S6E). Since the 700 kb fragment (from putative 5′ enhancer to 3′ UTR) of *ank3* genomic DNA was not readily suitable for BAC/YAC transgenesis, we next transfected pGL3 dual Firefly and Renilla luciferase reporters into pRGP cultures, which showed that both the 5′ and 3′ genomic fragments can function as transcriptional enhancers in pRGPs (Figure 5G). To determine if Foxj1 binds directly to these *ank3* sites, we performed chromatin immunoprecipitation (ChIP) experiments with Myc antibody on pRGPs infected with lentivirus expressing Foxj1-Myc. Using DNA primers specific to the *ank3* 5′ and 3′ enhancers, we showed by PCR after ChIP that Foxj1-Myc was able to bind to these genomic sequences in pRGPs (Figure 5H).

### Transitioning of RC2+ radial glia into postnatal NSCs without ependymal niche formation

With the absence of Ank3 expression, we wondered if a primary defect in Foxj1 cKO pRGPs was an inability to self-cluster, and thus unable to assemble proper SVZ architecture. Under time-lapse live imaging of Foxj1-GFP+ pRGPs in ependymal clustering assays, we saw that while pRGPs cultured from littermate controls were indistinguishable from wild-type cells (Movie S2 and data not shown), the Foxj1 cKO pRGPs uniformly failed to organize into clusters, and remained positionally static after expansion (Movie S4 and Figure 6A). We employed standardized thresholding (Figure S7A) to quantify this significant clustering defect in cKO pRGPs (Figure 6B).

It is not known whether radial glial transition into postnatal SVZ NSCs is niche dependent, or cell-intrinsically regulated. Since these primary defects in ependymal maturation and assembly have prevented formation of the SVZ niche postnatally in Foxj1 cKO mice, we next wanted to see if pRGPs destined to becoming SVZ NSCs can still make their transition. IHC staining for radial glial marker RC2 showed that while it was highly expressed by the developing SVZ at P2 in both the control and cKO mice, this expression was properly down-regulated by P6 in both genotypes (Figure 6C). Ki67 staining on P6 brain sections showed no measurable differences on cellular proliferation at the ventricular surface between control and cKO mice (Figures 6D). Furthermore, anti-Caspase-3 staining at the same age also showed no noticeable increase in apoptosis in the cKO mice (Figure S7B), suggesting RC2+ radial glia had transitioned into postnatal NSCs without ependymal niche formation.

To validate the presence of NSCs in this environment, we employed the adherent SVZ NSC culture assay (Scheffler et al., 2005) by harvesting primary cells from both P6 control and cKO mice. NSC cultures from the cKO lateral ventricular wall expanded in proliferation media like those from control mice (data not shown). Differentiation of passage 2 primary cultures showed abundant production of Tuj1+ neurons, GFAP+ astrocytes, and CNPase+

oligodendrocytes from both the control and cKO cultures, with quantification detecting no appreciable differences in lineage-restricted differentiation potential (Figure 6E and data not shown). These results are consistent with the notion that SVZ ependymal niche formation was not required for RC2$^+$ radial glia to transition into RC2$^-$ postnatal NSCs. However, the onset of hydrocephalus after 1 week of age in cKO mice prevented us from drawing further conclusions about SVZ niche function on neurogenesis.

### Inducible disruption of SVZ ependymal niche leads to depletion of neuroblast chains

Previously, it had not been possible to inducibly remove SVZ ependymal structure in vivo to directly demonstrate its functional significance on neurogenesis. Since we showed that the Foxj1-Ank3 pathway was required for SVZ formation, our strategy was to use the *foxj1-CreER$^{t2}$* transgene (Figure S3A) to disrupt this pathway in the SVZ after it had assembled properly. We generated *foxj1-CreER$^{t2}$; foxj1$^{KO/Flox}$* (inducible KO, iKO) mice by crossing *foxj1-CreER$^{t2}$; foxj1$^{KO/+}$* and *foxj1$^{Flox/Flox}$* animals. We did not observed histologic or phenotypic differences between *foxj1-CreER$^{t2}$; foxj1$^{Flox/+}$* littermate controls injected with tamoxifen and non-injected iKO mice (data not shown). For experiments, we administered single-dose tamoxifen at P14, and harvested brains at P28 to study the effects on SVZ and new neuron production. IHC staining on coronal sections from tamoxifen-injected control and iKO littermates showed that we were able to inducibly remove Ank3 expression from the ventricular surface (Figure S8A). Consistent with our previous observations, after in vivo Ank3 knockdown (Figure 3E), as well as in *nestin-Cre; foxj1$^{KO/Flox}$* mice (Figure 4D), inducible removal of Foxj1 and Ank3 also resulted in increased Glast and decreased S100β expression on the ventricular surface (Figure S8B). To confirm tamoxifen-mediated deletion of *foxj1*, we crossed into the iKO background a Rosa26-tdTomato reporter line (*r26r-tdTomato*). IHC staining of brain sections from *foxj1-CreER$^{t2}$, foxj1$^{KO/Flox}$; r26r-tdTomato$^{Flox/+}$* mice, 5 days after tamoxifen injection, showed that while there were rare tdTomato$^+$ ependymal cells retaining some Foxj1 (likely due to transient nature of CreER-mediated recombination), most tdTomato$^+$ cells had downregulated Foxj1 expression (Figure S8C).

To see how these structural disruptions in the mature niche may affect SVZ neurogenesis, we performed wholemount IHC staining using antibodies against DCX, Ank3, and Acetylated-tubulin. We used coordinate-stitching confocal software to acquire Z-stack images over the entire ventricular surface, which allowed us to simultaneously assess Ank3 / multicilia status and their relationships to newborn neuroblasts traveling in chains beneath the ventricular surface. Confocal images of DCX staining from control P28 mouse ventricular surface revealed robust migratory chains of neuroblasts (Figure 7A). In contrast, iKO mice injected with tamoxifen at P14 and sacrificed at P28 showed significant defects in the coverage of neuroblast chains along the ventricular wall (Figures 7B and 7C). Since the Foxj1-CreER$^{t2}$ targeting strategy generated mosaic populations of mutant and unaffected ependymal cells, we were able to largely avoid the appearance of hydrocephalus harvesting brains 2 weeks after tamoxifen injection (Figure 7B). In some animals we did observe hydrocephalus, as indicated by the enlargement of ventricular surface during tissue harvesting, and this phenotype correlated with extensive removal of ependymal Ank3 expression as confirmed by IHC staining and confocal analysis (Figures 7C and 7D).

We inverted the darkfield wholemount DCX neuroblast images and noted in red, areas where we observed continuous patches of Ank3 defects (accompanying Figures 7B and 7C). After analysis in several tamoxifen injected iKO mice, we could not find intact DCX$^+$ migratory chains in areas that showed extensive ependymal Ank3 loss (Figures 7B, 7C, and data not shown). We observed that on the borders between unaffected ependymal regions and cells with depleted Ank3 expression, DCX$^+$ neuroblast chains became disrupted (Figures 7D and S8D). Predictably, these defects along the ventricular wall led to significant

decrease in cellularity/size of the rostral migratory stream (RMS) in P28 olfactory bulbs after P14 tamoxifen induction (Figure 7E). It is interesting to note that 2 weeks after tamoxifen injection, Ank3 expression was often more affected from Foxj1 deletion than surface multicilia, perhaps reflecting the relative turnover rates of each in mature ependymal cells (Figures 7D and S8C). Consistent with the dramatic reduction in DCX$^+$ neuroblasts, Ki67 staining on coronal sections where large areas of ependyma were targeted showed decreased SVZ proliferation (Figure S8E).

To understand whether the iKO phenotypes may be partly due to inducible targeting of SVZ NSCs, we performed lineage-tracing experiments in *foxj1-CreER$^{t2}$; r26r-tdTomato* mice. We reasoned that if Foxj1-CreER$^{t2}$ can mediate significant recombination in mature SVZ NSCs after niche formation, we should see tdTomato$^+$ lineage-traced neuroblast chains along the ventricular wall. After tamoxifen induction at P14, wholemount IHC staining from P28 *foxj1-CreER$^{t2}$; r26r-tdTomato* lateral ventricular walls showed abundant tdTomato$^+$ ependymal cells (Figure S8F). However, we could not detect significant co-expression of tdTomato in DCX$^+$ neuroblasts in these mice (Figure S8F), in contrast to identically treated *nestin-CreER$^{tm}$; r26r-tdTomato* animals. We performed 3D-colocalization analyses on wholemounts from multiple animals to quantify this significant difference in tdTomato$^+$DCX$^+$ labeling (Figure S8H). Any colocalization in *foxj1-CreER$^{t2}$; r26r-tdTomato* wholemounts were observed mostly from the dorsal ventricular edge, where individual cells within dense neuroblast chains were difficult to resolve. We therefore performed live imaging of these dense neuroblast chains from P28 ventricular wholemounts after P14 tamoxifen induction, which revealed little tdTomato$^+$ migrating cells from *foxj1-CreER$^{t2}$; r26r-tdTomato* wholemounts, in contrast to identically treated and imaged *nestin-CreER$^{tm}$; r26r-tdTomato* samples (Movie S5). These results showed that our Foxj1-CreER$^{t2}$ line does not significantly target the mature SVZ NSC population along the ventricular wall (this specificity may differ between CreER transgenes). Our results also demonstrated that ependymal niche cells, although derived from radial glia, once mature do not contribute significantly to new neuron production. Thus the role for FoxJ1 appears to be limited to periods after the radial glia have committed to a niche cell fate, and are no longer in the stem cell lineage.

## Ank3 expression in niche clusters is required for new neuron production

Within targeted ependymal regions down-regulating Ank3 expression in iKO mice, concurrent with the loss of neuroblast chains, we also saw formation of GFAP$^+$ clusters (Figure 8A). To explore the possibility that ependymal Ank3 expression is directly required for SVZ NSCs to generate new neurons, we first wanted to address whether Ank3 is cell-intrinsically required by SVZ NSCs to make neuroblasts. We again used the adherent SVZ NSC culture assay from wild-type P5 mice, and infected early passage proliferating cultures with lentivirus expressing Ank3 shRNA (Figures 3C and S4A) and GFP driven by a ubiquitous EF1α promoter. There was no noticeable difference in the proliferative capacities of SVZ NSCs between cultures infected with control versus Ank3 shRNA lentiviruses (data not shown), since these cells are Ank3-negative (Figure 1). Upon in vitro differentiation, we saw abundant GFP$^+$DCX$^+$ neuroblasts that persisted for the duration of culture in both the control and Ank3 shRNA infected cultures (Figure 8B and data not shown), showing that Ank3 knockdown does not cell-intrinsically inhibit neuroblast production from SVZ NSCs. Consistent with the in vitro findings, we transplanted these Ank3 shRNA infected NSCs back in vivo, and observed 7 and 28 days post transplantation GFP$^+$ cells within the SVZ as well as neuroblasts and neurons in the RMS and olfactory bulb (Figure 8C). Quantification of GFP$^+$ cell numbers showed no obviously differences between control and Ank3 shRNA virus-treated transplantation experiments (data not shown).

We next tested the relationship between Ank3 and neuroblast production in our pRGP niche culture assay. Although no exogenous growth factors (EGF and bFGF, required for SVZ NSC renewal ex vivo) were added at any time to these primary cultures, we reasoned that perhaps the presence of Ank3+ ependymal niche cells may support NSCs and allow them to make neuroblasts during differentiation. IHC staining of pRGP culture in differentiation media 5 days after plating showed large numbers of DCX+ neuroblast clusters, with most in close proximity to Ank3+ niche clusters (arrows, Figure 8D). To determine if Ank3 expression by these niche clusters was required for neuroblast production, we used the same shRNA strategy to efficiently remove Ank3 protein expression from differentiating pRGPs (Figures 3C and S4B). This resulted in a dramatic reduction of DCX+ neuroblast clusters seen in Ank3 shRNA-treated versus control virus-treated cultures (Figures 8E). Harvesting the Ank3 shRNA-treated pRGP cultures earlier or later during differentiation also did not show formation of DCX+ neuroblast clusters (data not shown), revealing that the defects in neuroblast production were not due to DCX+ cells dying or a delay in differentiation program. These results are in support of our in vivo observations that postnatal Ank3-mediated SVZ ependymal niche organization is required for the continued production of new neurons.

## DISCUSSION

To study the functional significance of SVZ niche on new neuron production, we first showed that pRGPs have an intrinsic ability to cluster into structures of the adult SVZ neurogenic niche. We discovered that the lateral membrane adapter protein Ank3 is specifically upregulated in pRGPs destined to become SVZ niche cells, but not in stem cells, and that this Foxj1-regulated expression is necessary for pRGP assembly into mature SVZ structures. Disruption of this Foxj1-Ank3 pathway in vivo specifically removed SVZ architecture, allowing us to demonstrate for the first time that the mature ependymal niche is required to maintain continued production of new neurons in the postnatal brain.

### Ank3 and postnatal radial glial lateral membrane specialization

Our results showing that Ank3 functions in pRGPs destined to become SVZ ependymal cells, but not in future stem cells, revealed selective Ankyrin usage by a subpopulation of progenitors to establish brain ventricular wall organization. This previously undescribed function for Ankyrin is exciting both for SVZ neurogenesis and Ankyrin biology. The *ankyrin* gene family was first discovered over 30 years ago, but until this study no transcription factor had been linked to these proteins. While we showed here that pRGPs upregulate the 190 kD isoforms of Ank3, mature neurons express the larger 480 and 270 kD Ank3 isoforms (Kordeli et al., 1995). Thus far we have not detected Foxj1 expression in mature Ank3+ neurons, suggesting separate transcriptional networks regulating Ank3 expression in neurons versus pRGPs. Foxj1 is a well-known regulator of multicilia formation, but our results here, as well as those from previous studies (Lin et al., 2004; Jacquet et al., 2009) show that there are other important functions for this protein. A microarray study by Ghashghaei and colleagues in search of additional downstream molecules regulated by Foxj1 did not identify Ank3 or other transcription factors (Jacquet et al., 2009). We believe further experiments using expression profiling will be needed to understand which proteins may work together with Foxj1 to regulate Ank3 expression in pRGPs generating the adult SVZ neurogenic niche.

Beyond pRGP cell-cell adhesion, are there other molecules anchored by Ank3 that facilitate SVZ niche generation? Prior to growing multicilia at their apical surfaces, pRGPs begin to interdigitate their lateral membranes with neighboring niche progenitors. Although the significance of this elaborate cellular transformation is currently unknown, it is possible that it goes beyond simple sealing of the epithelium. One intriguing class of Ankyrin-associated

proteins that warrant further investigation is voltage-gated ion channels. Ank3 is known to physically associate with both voltage-gated sodium, as well as voltage-gated potassium channels (Bennett and Healy, 2008). It would be of interest to examine whether these channels are involved in the formation/maintenance of adult SVZ niche.

## SVZ niche architecture and production of new neurons

To demonstrate functional significance of SVZ architecture on the production of new neurons in postnatal and adult rodent brains, it is necessary to specifically disrupt niche cell function without targeting SVZ NSCs. These experiments may seem conceptually straightforward, but have been technically challenging due to our lack of understanding of how the SVZ niche is generated. They are made more difficult by the fact that ependymal niche cell defects can result in significant secondary phenotypes that preclude direct assessment of niche function on neurogenesis, such as what we observed previously with postnatal Numb deletion (Kuo et al., 2006). Our identification of Ank3 expression regulated by Foxj1 in SVZ niche progenitors gave us new traction, as we were aided by the relatively normal ventricular size, and structurally intact ventricular wall surfaces in our mutant mice postnatally. The delay in onset of hydrocephalus also proved useful for demonstrating the roles for SVZ architecture on radial glial transition, as well as new neuron production after inducible removal of niche organization.

It had been shown that SVZ stem cells are derived from RC2$^+$ embryonic radial glia (Merkle et al., 2004), although little is currently known about the molecular pathways regulating this developmental switch. These pRGPs transition from a Nestin$^+$RC2$^+$GFAP$^-$ phenotype at P0 to a Nestin$^+$RC2$^-$GFAP$^+$ phenotype by P14 (Tramontin et al., 2003). As Nestin is expressed by mature ependymal cells as well as SVZ niche progenitors, currently there is a lack of better biomarkers to assist in the identification of pRGPs destined to becoming SVZ stem cells. We showed that in the absence of postnatal ependymal maturation, there was still proper down-regulation of RC2 expression, suggesting that embryonic radial glia did not persist in the cKO SVZ postnatally. Normal SVZ proliferation in vivo, the lack of increased cell death, and proper differentiation of SVZ stem cell cultures in vitro from P6 cKO mice are all consistent with the notion that radial glial differentiation into SVZ stem cells does not require proper ependymal niche assembly. Work in *Drosophila* neural progenitors has demonstrated that the control of progenitor maturation over time can be precisely controlled by cell-intrinsic transcriptional programs (Isshiki et al., 2001; Maurange et al., 2008). It will be of interest to understand whether similar mechanisms exist during pRGP differentiation into SVZ NSCs.

Once the SVZ neurogenic niche is formed, our results showed that the continued production of new neurons migrating in chains along the ventricular wall required intact ependymal organization. To our knowledge, this represents the first demonstration of such functional requirement for the SVZ ependymal niche. Ideally, this would allow us to address the effects of newborn neuron depletion from the SVZ on olfactory bulb (OB) circuitry and brain homeostasis. However, those experiments are difficult to perform due to the nature of inducible CreER method, generating mosaic cell populations in vivo. In our study, we struck a balance between targeting enough SVZ niche cells to show neuroblast production deficits, and targeting too many resulting in hydrocephalus. One way to study long-term consequences of depleting new neuron from the SVZ may be to rethink strategies for generating Ank3 mutant mice. Our identification of a critical role for Ank3 and the ependymal niche in maintaining new neuron production from adult NSCs should synergize with future studies on generating new neurons in the adult brain in health and disease.

## EXPERIMENTAL PROCEDURES

### Cell culture

pRGP differentiation from P0 mice: lateral ventricular wall was dissected, triturated in DMEM-High Glucose 4.5 (GIBCO), 10% FBS (Hyclone), 1% L-glutamine, 1% Pen/Strep, and plated at 450-500,000 cells / ml in the same media on Poly-D-Lysine (Sigma) coated surface, incubated under normal cell culture conditions. When cells reach 90-100% confluence (3 to 4 days after plating) media was switched to 2% FBS (other ingredients same as above) and not changed again for the duration of experiment. Adherent SVZ NSC culture was performed as described (Scheffler et al., 2005).

### Electron microscopy and immunohistochemical staining

Details on electron microscopy, immunohistochemical staining, and antibodies used can be found in supplemental information online.

### Imaging and analysis

Time-lapse culture experiments were acquired on inverted Zeiss Cell Observer System under standard environmental control. All IHC images were acquired on Leica TCS SP5 confocal microscope, with control and experimental samples imaged under identical settings. Details can be found in supplemental information online.

### Lentiviral experiments

Lentiviruses were produced in 293T17 cells through triple-transfection of transfer plasmids (pLVTHM or pWPXL), psPAX2, and pMD2.G. Mouse Ank3 was targeted for shRNA knockdown through the sequence GAGAGAGAACTTATCGTCC cloned into pSuper-GFP, then subcloned into lentiviral plasmid pLVTHM. EF-1α promoter in pLVTHM driving GFP expression was replaced by 1 kb human Foxj1 promoter (Ostrowski et al., 2003). A human Ank3 shRNA (Kizhatil and Bennett, 2004) cloned into pLVTHM was used as off-target effect control for pRGP culture experiments. 3′ Myc-tag Foxj1 cDNA and 190 kD Ank3 cDNA were independently cloned into pWPXL lentiviral plasmid and driven under EF-1α promoter.

### Generation of *foxj1-flox* mice

Details of gene targeting strategy and PCR genotyping protocol can be found in supplemental information online.

### In vivo injections

In vivo injection of lentivirus and was performed as described (Merkle et al., 2004). SVZ transplantation of passage 2 primary adherent SVZ stem cells was performed as described (Merkle et al., 2007) with modifications which can be found in supplemental information online. Tamoxifen (10 mg/ml, freshly dissolved in corn oil) was injected intraperitoneally at 0.15 mg per gram of body weight to induce CreER$^{t2}$-mediated recombination.

### Biochemical assays and sequence analysis

Details on Western blots, gel shifts, ChIP assays, and enhancer analyses can be found in supplemental information online.

## Supplementary Material

Refer to Web version on PubMed Central for supplementary material.

## Acknowledgments

## REFERENCES

Abdi KM, Bennett V. Adducin promotes micrometer-scale organization of beta2-spectrin in lateral membranes of bronchial epithelial cells. Mol Biol Cell. 2008; 19:536–545. [PubMed: 18003973]

Alvarez-Buylla A, Lim DA. For the long run: maintaining germinal niches in the adult brain. Neuron. 2004; 41:683–686. [PubMed: 15003168]

Badis G, Berger MF, Philippakis AA, Talukder S, Gehrke AR, Jaeger SA, Chan ET, Metzler G, Vedenko A, Chen X, et al. Diversity and complexity in DNA recognition by transcription factors. Science. 2009; 324:1720–1723. [PubMed: 19443739]

Bejerano G, Siepel AC, Kent WJ, Haussler D. Computational screening of conserved genomic DNA in search of functional noncoding elements. Nat Methods. 2005; 2:535–545. [PubMed: 16170870]

Bennett V, Healy J. Organizing the fluid membrane bilayer: diseases linked to spectrin and ankyrin. Trends Mol Med. 2008; 14:28–36. [PubMed: 18083066]

Brody SL, Yan XH, Wuerffel MK, Song SK, Shapiro SD. Ciliogenesis and left-right axis defects in forkhead factor HFH-4-null mice. Am J Respir Cell Mol Biol. 2000; 23:45–51. [PubMed: 10873152]

Carlen M, Meletis K, Goritz C, Darsalia V, Evergren E, Tanigaki K, Amendola M, Barnabe-Heider F, Yeung MS, Naldini L, et al. Forebrain ependymal cells are Notch-dependent and generate neuroblasts and astrocytes after stroke. Nat Neurosci. 2009; 12:259–267. [PubMed: 19234458]

Doetsch F, Caille I, Lim DA, Garcia-Verdugo JM, Alvarez-Buylla A. Subventricular zone astrocytes are neural stem cells in the adult mammalian brain. Cell. 1999; 97:703–716. [PubMed: 10380923]

Gotz M, Huttner WB. The cell biology of neurogenesis. Nat Rev Mol Cell Biol. 2005; 6:777–788. [PubMed: 16314867]

Guirao B, Meunier A, Mortaud S, Aguilar A, Corsi JM, Strehl L, Hirota Y, Desoeuvre A, Boutin C, Han YG, et al. Coupling between hydrodynamic forces and planar cell polarity orients mammalian motile cilia. Nat Cell Biol. 2010; 12:341–350. [PubMed: 20305650]

Isshiki T, Pearson B, Holbrook S, Doe CQ. Drosophila neuroblasts sequentially express transcription factors which specify the temporal identity of their neuronal progeny. Cell. 2001; 106:511–521. [PubMed: 11525736]

Jacquet BV, Salinas-Mondragon R, Liang H, Therit B, Buie JD, Dykstra M, Campbell K, Ostrowski LE, Brody SL, Ghashghaei HT. FoxJ1-dependent gene expression is required for differentiation of radial glia into ependymal cells and a subset of astrocytes in the postnatal brain. Development. 2009; 136:4021–4031. [PubMed: 19906869]

Karolchik D, Bejerano G, Hinrichs AS, Kuhn RM, Miller W, Rosenbloom KR, Zweig AS, Haussler D, Kent WJ. Comparative genomic analysis using the UCSC genome browser. Methods Mol Biol. 2007; 395:17–34. [PubMed: 17993665]

Kelsch W, Sim S, Lois C. Watching synaptogenesis in the adult brain. Annual review of neuroscience. 2010; 33:131–149.

Kizhatil K, Bennett V. Lateral membrane biogenesis in human bronchial epithelial cells requires 190-kDa ankyrin-G. J Biol Chem. 2004; 279:16706–16714. [PubMed: 14757759]

Kizhatil K, Davis JQ, Davis L, Hoffman J, Hogan BL, Bennett V. Ankyrin-G is a molecular partner of E-cadherin in epithelial cells and early embryos. J Biol Chem. 2007; 282:26552–26561. [PubMed: 17620337]

Kokovay E, Goderie S, Wang Y, Lotz S, Lin G, Sun Y, Roysam B, Shen Q, Temple S. Adult SVZ lineage cells home to and leave the vascular niche via differential responses to SDF1/CXCR4 signaling. Cell Stem Cell. 2010; 7:163–173. [PubMed: 20682445]

Kokovay E, Shen Q, Temple S. The incredible elastic brain: how neural stem cells expand our minds. Neuron. 2008; 60:420–429. [PubMed: 18995816]

Kordeli E, Lambert S, Bennett V. AnkyrinG. A new ankyrin gene with neural-specific isoforms localized at the axonal initial segment and node of Ranvier. J Biol Chem. 1995; 270:2352–2359. [PubMed: 7836469]

Kriegstein A, Alvarez-Buylla A. The glial nature of embryonic and adult neural stem cells. Annu Rev Neurosci. 2009; 32:149–184. [PubMed: 19555289]

Kuo CT, Mirzadeh Z, Soriano-Navarro M, Rasin M, Wang D, Shen J, Sestan N, Garcia-Verdugo J, Alvarez-Buylla A, Jan LY, et al. Postnatal deletion of Numb/Numblike reveals repair and remodeling capacity in the subventricular neurogenic niche. Cell. 2006; 127:1253–1264. [PubMed: 17174898]

Lim L, Zhou H, Costa RH. The winged helix transcription factor HFH-4 is expressed during choroid plexus epithelial development in the mouse embryo. Proc Natl Acad Sci U S A. 1997; 94:3094–3099. [PubMed: 9096351]

Lin L, Spoor MS, Gerth AJ, Brody SL, Peng SL. Modulation of Th1 activation and inflammation by the NF-kappaB repressor Foxj1. Science. 2004; 303:1017–1020. [PubMed: 14963332]

Lledo PM, Merkle FT, Alvarez-Buylla A. Origin and function of olfactory bulb interneuron diversity. Trends Neurosci. 2008; 31:392–400. [PubMed: 18603310]

Luo J, Shook BA, Daniels SB, Conover JC. Subventricular zone-mediated ependyma repair in the adult mammalian brain. J Neurosci. 2008; 28:3804–3813. [PubMed: 18385338]

Marszalek JR, Liu X, Roberts EA, Chui D, Marth JD, Williams DS, Goldstein LS. Genetic evidence for selective transport of opsin and arrestin by kinesin-II in mammalian photoreceptors. Cell. 2000; 102:175–187. [PubMed: 10943838]

Maurange C, Cheng L, Gould AP. Temporal transcription factors and their targets schedule the end of neural proliferation in Drosophila. Cell. 2008; 133:891–902. [PubMed: 18510932]

Merkle FT, Mirzadeh Z, Alvarez-Buylla A. Mosaic organization of neural stem cells in the adult brain. Science. 2007; 317:381–384. [PubMed: 17615304]

Merkle FT, Tramontin AD, Garcia-Verdugo JM, Alvarez-Buylla A. Radial glia give rise to adult neural stem cells in the subventricular zone. Proc Natl Acad Sci USA. 2004; 101:17528–17532. [PubMed: 15574494]

Miller FD, Gauthier-Fisher A. Home at last: neural stem cell niches defined. Cell Stem Cell. 2009; 4:507–510. [PubMed: 19497279]

Mirzadeh Z, Merkle FT, Soriano-Navarro M, Garcia-Verdugo JM, Alvarez-Buylla A. Neural stem cells confer unique pinwheel architecture to the ventricular surface in neurogenic regions of the adult brain. Cell Stem Cell. 2008; 3:265–278. [PubMed: 18786414]

Ostrowski LE, Hutchins JR, Zakel K, O'Neal WK. Targeting expression of a transgene to the airway surface epithelium using a ciliated cell-specific promoter. Mol Ther. 2003; 8:637–645. [PubMed: 14529837]

Prothmann C, Wellard J, Berger J, Hamprecht B, Verleysdonk S. Primary cultures as a model for studying ependymal functions: glycogen metabolism in ependymal cells. Brain Res. 2001; 920:74–83. [PubMed: 11716813]

Rawlins EL, Ostrowski LE, Randell SH, Hogan BL. Lung development and repair: contribution of the ciliated lineage. Proc Natl Acad Sci U S A. 2007; 104:410–417. [PubMed: 17194755]

Sawamoto K, Wichterle H, Gonzalez-Perez O, Cholfin JA, Yamada M, Spassky N, Murcia NS, Garcia-Verdugo JM, Marin O, Rubenstein JL, et al. New neurons follow the flow of cerebrospinal fluid in the adult brain. Science. 2006; 311:629–632. [PubMed: 16410488]

Scheffler B, Walton NM, Lin DD, Goetz AK, Enikolopov G, Roper SN, Steindler DA. Phenotypic and functional characterization of adult brain neuropoiesis. Proc Natl Acad Sci USA. 2005; 102:9353–9358. [PubMed: 15961540]

Shen Q, Wang Y, Kokovay E, Lin G, Chuang SM, Goderie SK, Roysam B, Temple S. Adult SVZ stem cells lie in a vascular niche: a quantitative analysis of niche cell-cell interactions. Cell Stem Cell. 2008; 3:289–300. [PubMed: 18786416]

Spassky N, Merkle FT, Flames N, Tramontin AD, Garcia-Verdugo JM, Alvarez-Buylla A. Adult ependymal cells are postmitotic and are derived from radial glial cells during embryogenesis. J Neurosci. 2005; 25:10–18. [PubMed: 15634762]

Suh H, Deng W, Gage FH. Signaling in adult neurogenesis. Annu Rev Cell Dev Biol. 2009; 25:253–275. [PubMed: 19575663]

Tavazoie M, Van der Veken L, Silva-Vargas V, Louissaint M, Colonna L, Zaidi B, Garcia-Verdugo JM, Doetsch F. A specialized vascular niche for adult neural stem cells. Cell Stem Cell. 2008; 3:279–288. [PubMed: 18786415]

Tramontin AD, Garcia-Verdugo JM, Lim DA, Alvarez-Buylla A. Postnatal development of radial glia and the ventricular zone (VZ): a continuum of the neural stem cell compartment. Cereb Cortex. 2003; 13:580–587. [PubMed: 12764031]

Tronche F, Kellendonk C, Kretz O, Gass P, Anlag K, Orban PC, Bock R, Klein R, Schutz G. Disruption of the glucocorticoid receptor gene in the nervous system results in reduced anxiety. Nat Genet. 1999; 23:99–103. [PubMed: 10471508]

Yu X, Ng CP, Habacher H, Roy S. Foxj1 transcription factors are master regulators of the motile ciliogenic program. Nat Genet. 2008; 40:1445–1453. [PubMed: 19011630]

Zhang Y, Huang G, Shornick LP, Roswit WT, Shipley JM, Brody SL, Holtzman MJ. A transgenic FOXJ1-Cre system for gene inactivation in ciliated epithelial cells. Am J Respir Cell Mol Biol. 2007; 36:515–519. [PubMed: 17255554]

Zhou D, Lambert S, Malen PL, Carpenter S, Boland LM, Bennett V. AnkyrinG is required for clustering of voltage-gated Na channels at axon initial segments and for normal action potential firing. J Cell Biol. 1998; 143:1295–1304. [PubMed: 9832557]
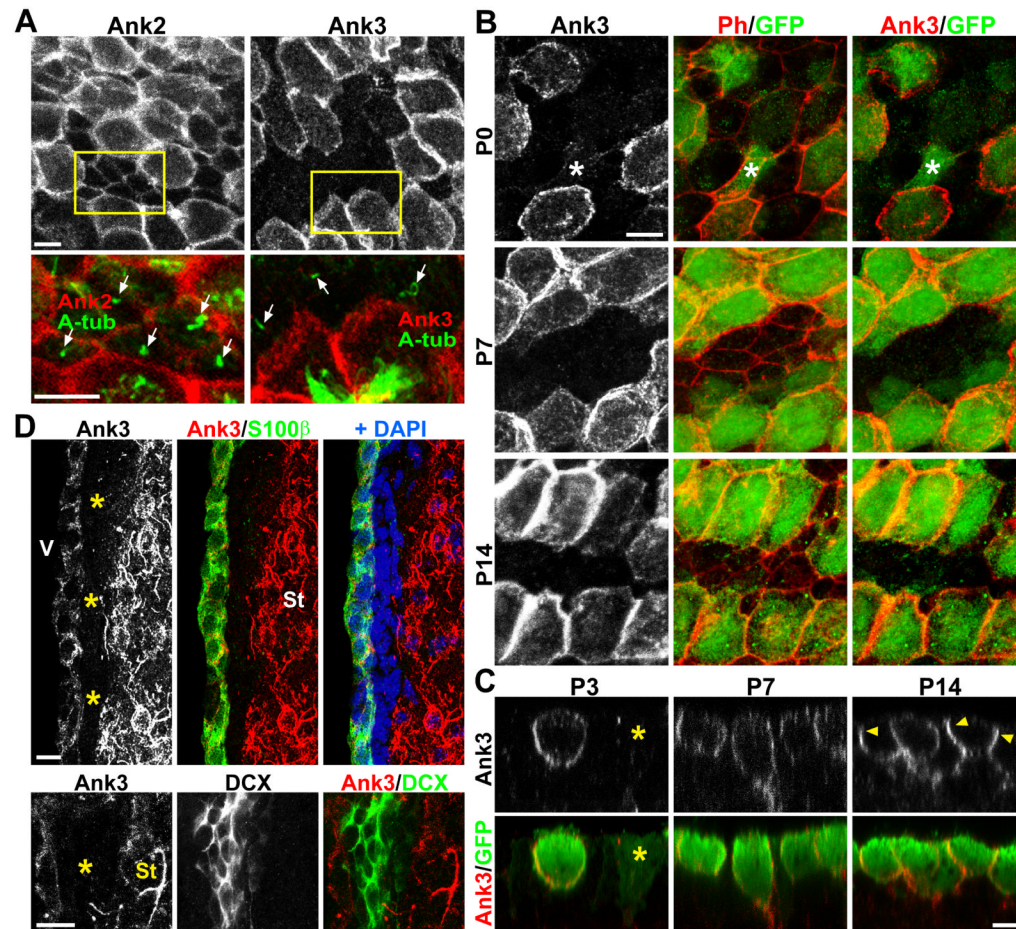
**Figure 1. Ank3 expression in SVZ neurogenic niche**

(A) IHC staining of P14 lateral ventricular wall wholemounts showing the specificity of Ank3 expression in multiciliated ependymal cells, but not monociliated cells (arrows). (B) Ank3 and GFP staining of brain lateral ventricular wall wholemounts from P0, P7, and P14 Foxj1-GFP transgenic mice. At P0, there were GFP+ pRGPs (smaller ventricular surface area) with low Ank3 expression (*). Ph = Phalloidin. (C) IHC staining of ventricular wall wholemounts in x-z plane, showing upregulation/lateral organization of Ank3 in Foxj1-GFP+ pRGPs during postnatal maturation (arrowheads). Note that GFP-dim cells at P3 did not have high Ank3 levels (*). (D) P14 coronal sections of SVZ stained with Ank3, S100β, DCX, DAPI, showing little to no Ank3 expression in DCX+ neuroblasts and SVZ beneath the ependyma (*). V: ventricle; St: striatum. Scale bar: (A – C) 5 μm, (D) 10 μm. See also Figure S1.
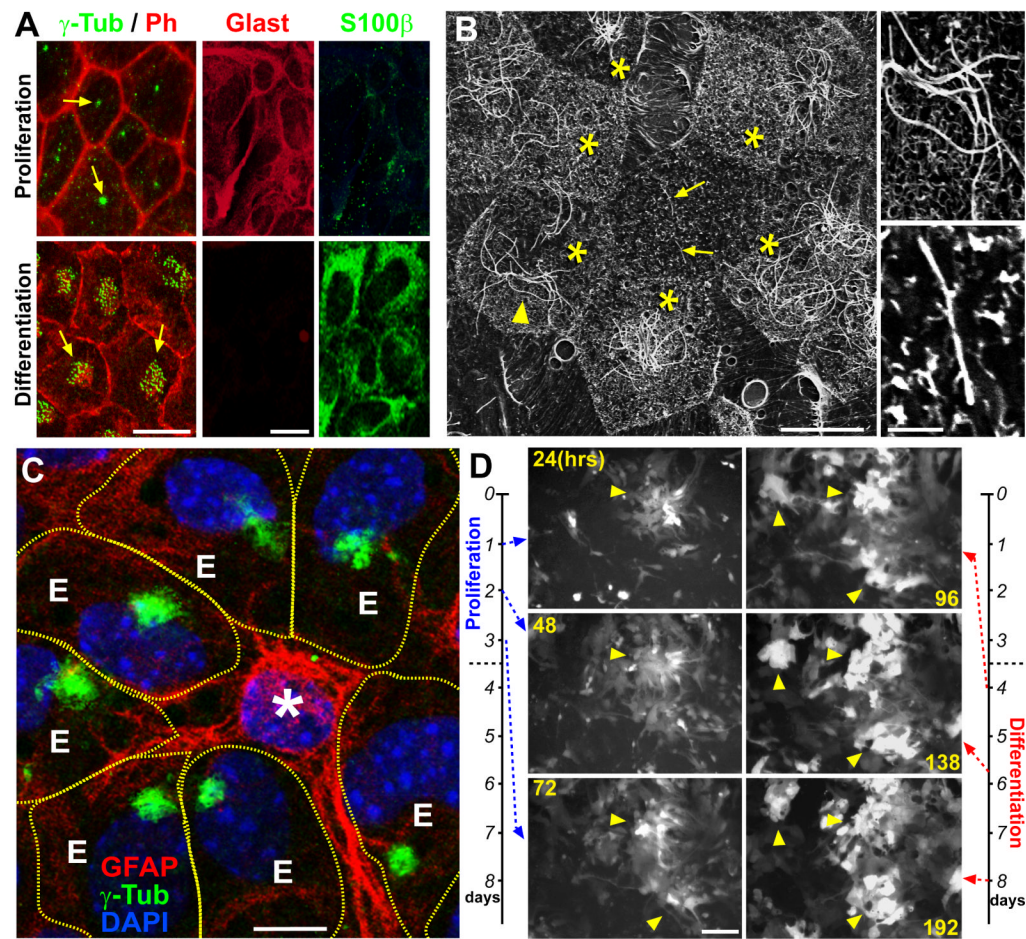
**Figure 2. In vitro generation of SVZ ependymal clusters**
(A) IHC staining of in vitro cultured pRGPs from P0 mice under proliferating (3 days after plating, upper row) and differentiating conditions (10 days after plating, bottom row). Note γ-Tubulin (γ-Tub) staining showing single basal body during proliferation (arrows, corresponding to monociliated cells), and multiple basal bodies per cell after differentiation (arrows, corresponding to multiciliated cells). (B) Scanning electron microscopic (SEM) images of differentiated pRGPs showing multiciliated ependymal cells (ECs, *) arranged in clusters around monociliated cells (arrows). Right panels show higher magnification view of multiciliated cell (arrowhead), and monociliated cells (arrows). (C) IHC staining of ependymal clusters. Monociliated cell in the center is GFAP$^+$ (*). Multiciliated ependymal cells show clustered γ-Tub staining (E), and their cell borders are represented by dash lines (traced from Phalloidin co-staining). (D) Stills from real-time live imaging movie of Foxj1-GFP$^+$ pRGPs showing proliferation and differentiation of SVZ progenitors. Note the increase in GFP$^+$ cell clustering during proliferation/differentiation transition (arrowheads, also see Movie S2). Scale bar: (A) 10 μm; (B) 10 μm / close-up 2 μm; (C) 5 μm; (D) 50 μm. See also Figure S2.
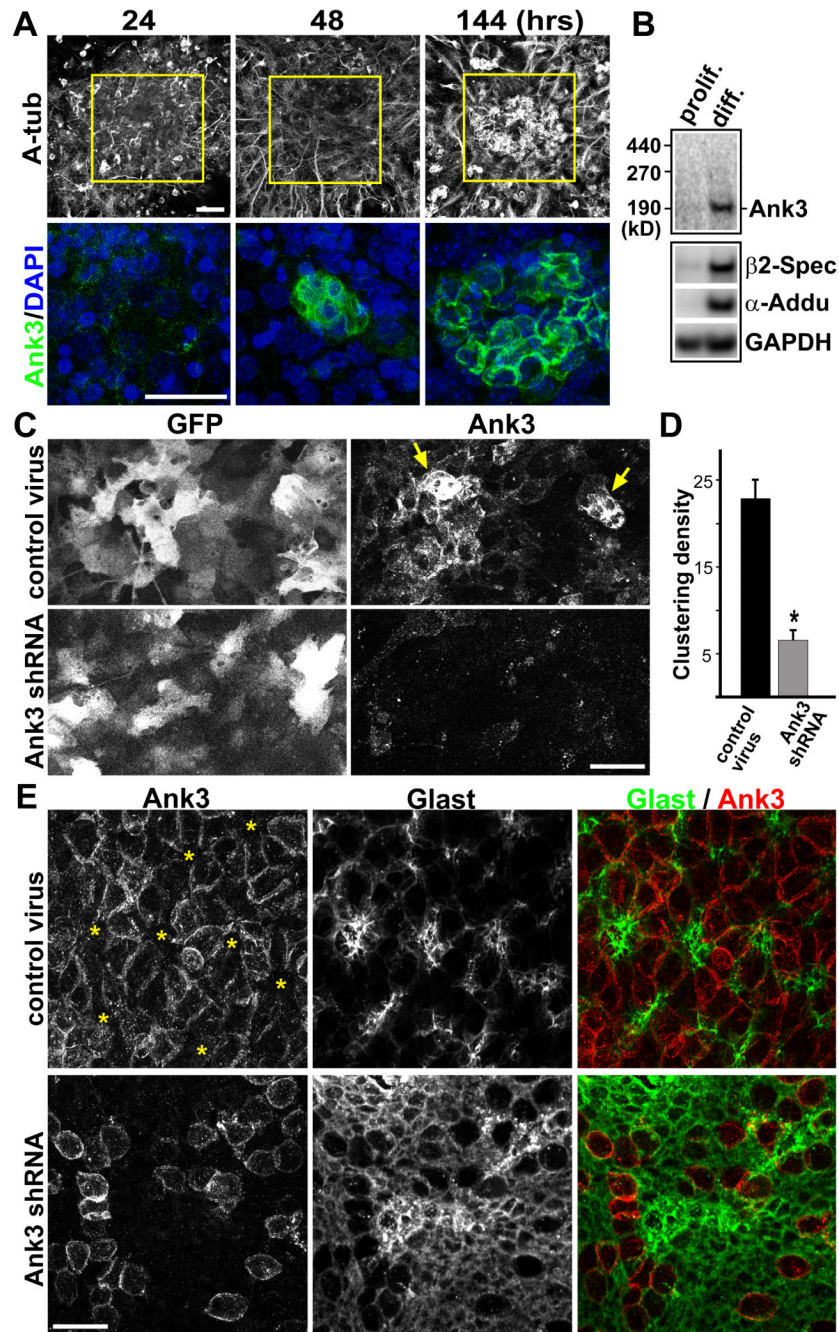
**Figure 3. Ank3 regulation of postnatal SVZ niche formation**
(A) IHC staining showing Ank3 upregulation in clusters during in vitro differentiation of pRGPs (hrs after plating). (B) Western-blot analyses of Ank3, β2-Spectrin, α-Adducin protein levels in pRGP culture under proliferating (3 days after plating) and differentiating conditions (8 days after plating). (C) Control and Ank3 shRNA lentiviral infection of pRGPs in culture, showing knock-down of Ank3 upregulation (arrows). Note the high infection efficiency. (D) Quantification of ependymal cluster formation in culture after lentiviral infection (see text and Figure S4B for details). * p < 0.05 Wilcoxon 2-sample test; error bar = sem; n = 5. (E) IHC staining of P5 ventricular wall wholemounts after P0 lentiviral-injection. Note that while Glast expression in control sample is largely concentrated to the

center of Ank3⁻ pinwheel-like structures (asterisks), after Ank3 knockdown most pRGPs still expressed high level of Glast, and showed disorganization (see also Figure S4C). Scale bar: (A, C, E) 20 μm. See also Figure S3 and S4.
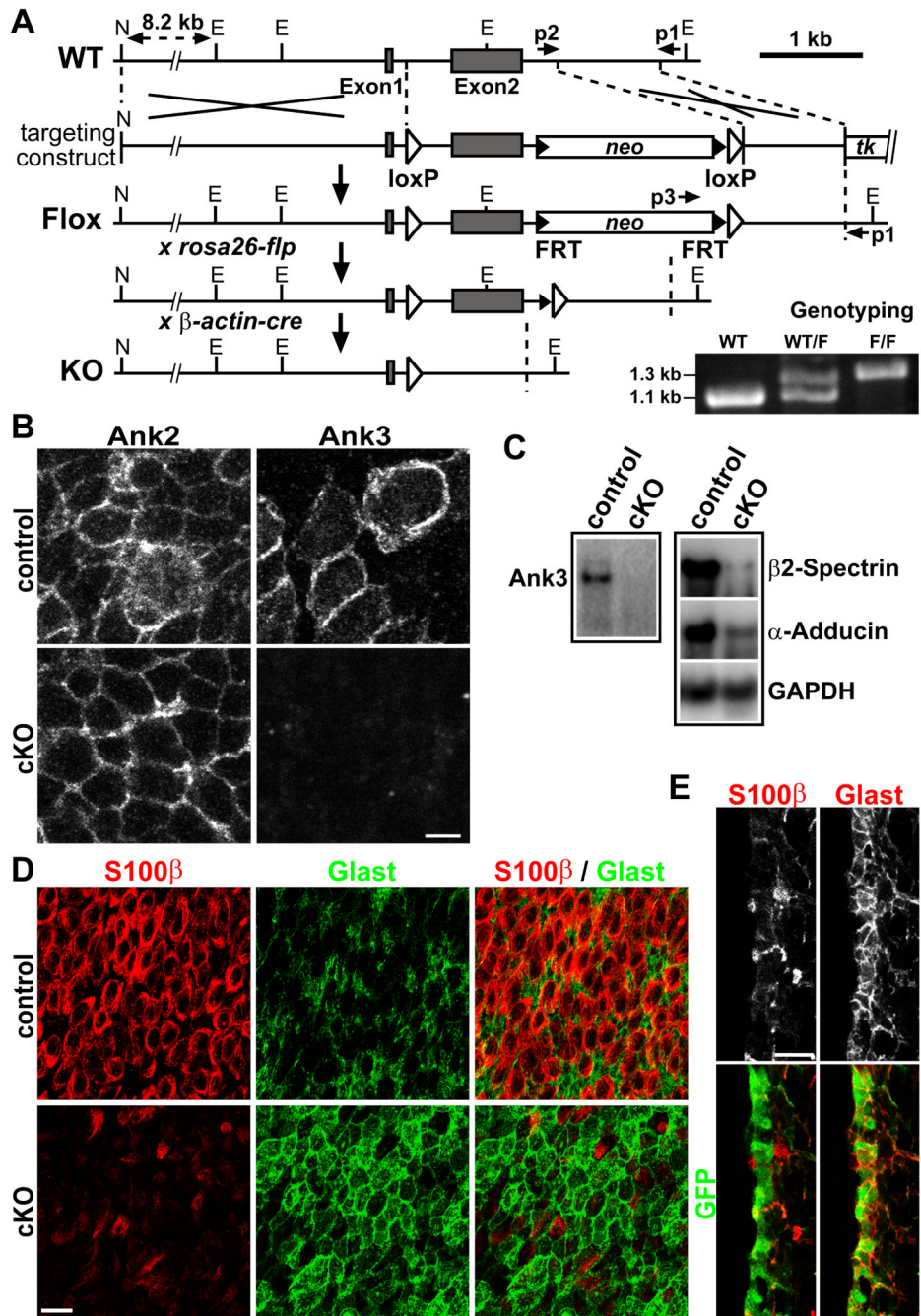
**Figure 4. Ank3 defects in conditional *foxj1* mutant mice**
(A) Schematic representation of the Foxj1-flox targeting strategy. N = NotI, E = EcoRI.
Germ-line transmission of Flox allele was verified by PCR genotyping using primers p1
(external to targeting construct), p2, and p3. Allele was crossed to *rosa26-flp*, removing
neomycin cassette for conditional Cre experiments; crossing to *β-actin-Cre* generated KO
allele. (B) IHC staining of P3 ventricular wall wholemounts from control and Foxj1 cKO
mice: note the lack of Ank3 expression in cKO pRGPs. (C) Western blot analyses of Ank3,
β2-Spectrin, α-Adducin protein levels in differentiated pRGPs from control and cKO mice.
(D) Lateral ventricular wall wholemount IHC staining from P6 control and cKO mice. (E)
IHC staining of lateral ventricular wall section from P6 cKO; Foxj1-GFP mice showing that

GFP$^+$ cells at the ventricular surface have low-S100β, but high-Glast expression. Scale bar: (B) 5 μm; (D, E) 20 μm. See also Figure S5.
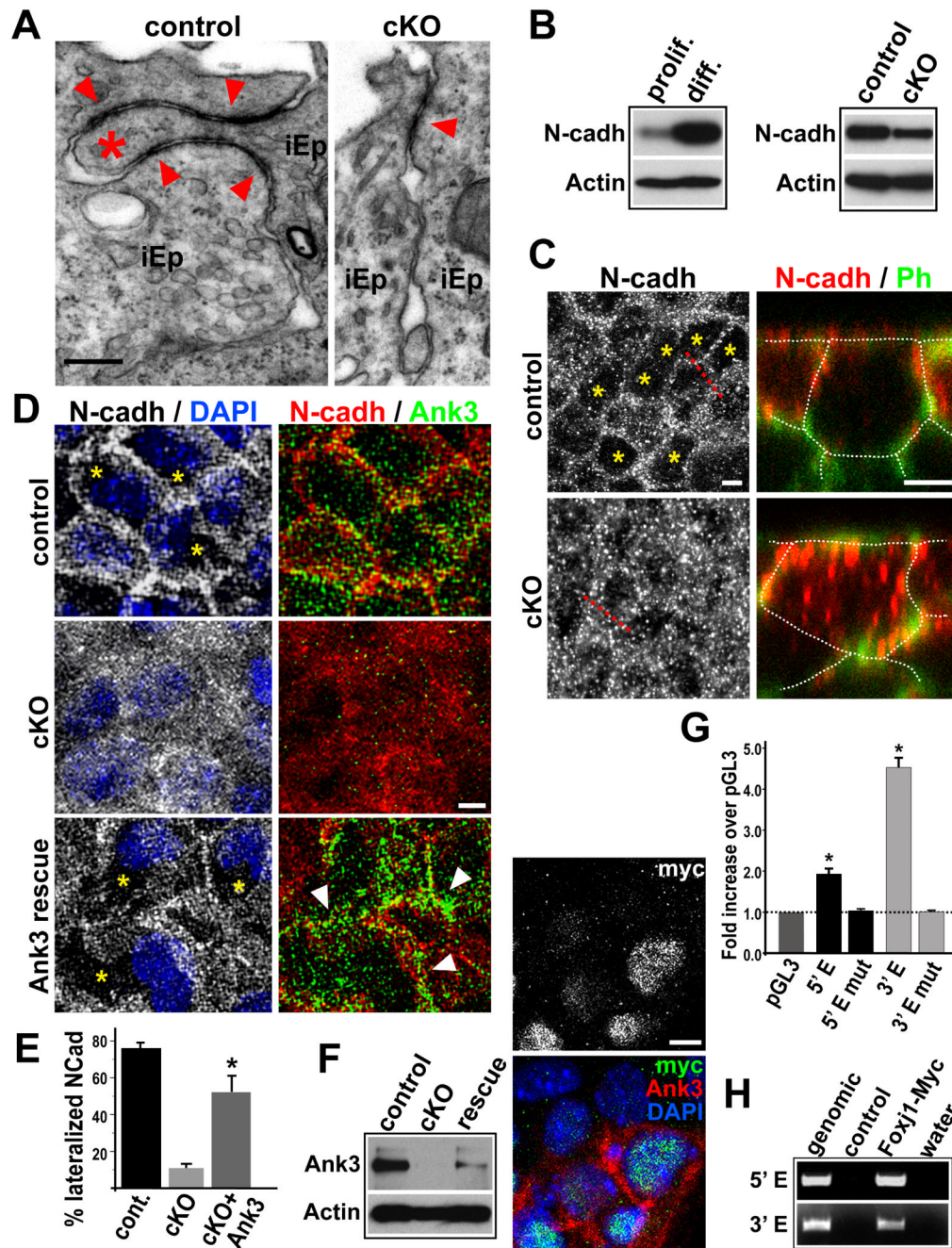
**Figure 5. Foxj1 regulation of Ank3 during SVZ niche formation**
(A) TEM of P4 ventricular wall lateral junctions between immature ependymal progenitors (iEp). Note the lack of interdigitation (*) / extension of apical adherens junctions (arrowheads) in cKO lateral borders. (B) Western blot analyses comparing N-cadherin expression levels during in vitro differentiation of pRGPs. (C) N-cadherin (N-cadh) IHC staining of P4 ventricular wall wholemounts in X-Y and X-Z planes. Cell borders visualized by Phalloidin (Ph) (traced by dashed lines for clarity). Ph and DAPI were used as landmarks to ensure cytoplasmic scanning in X-Z planes. (D) IHC analyses of N-cadherin expression in Foxj1 cKO pRGPs infected with lentivirus expressing 190 kD Ank3. Note the clearance of N-cadherin protein (*) from the cytoplasm of Foxj1 cKO pRGPs expressing Ank3

(arrowheads). (E) % of differentiated pRGP in culture with lateralized N-cadherin staining. In Foxj1 cKO rescue experiments, we assessed N-cadherin status in cells expressing infected Ank3. * p < 0.05 Wilcoxon 2-sample test; error bar = stdev.; n = 5. (F) Western blot and IHC analyses of Ank3 expression in cKO pRGPs infected with lentivirus expressing Foxj1-Myc. (G) Transcriptional activity of 5′ and 3′ enhancer elements assayed by luciferase constructs in pRGP cultures. * p < 0.001 Wilcoxon 2-sample test; error bar: sem; n = 6. (H) PCR primer amplification of 5′ Enh and 3′ Enh genomic DNA fragments after chromatin immunoprecipitation with Myc antibody from differentiated pRGPs. Scale bar: (A) 0.5 μm; (C, D, F) 5 μm. See also Figure S6.
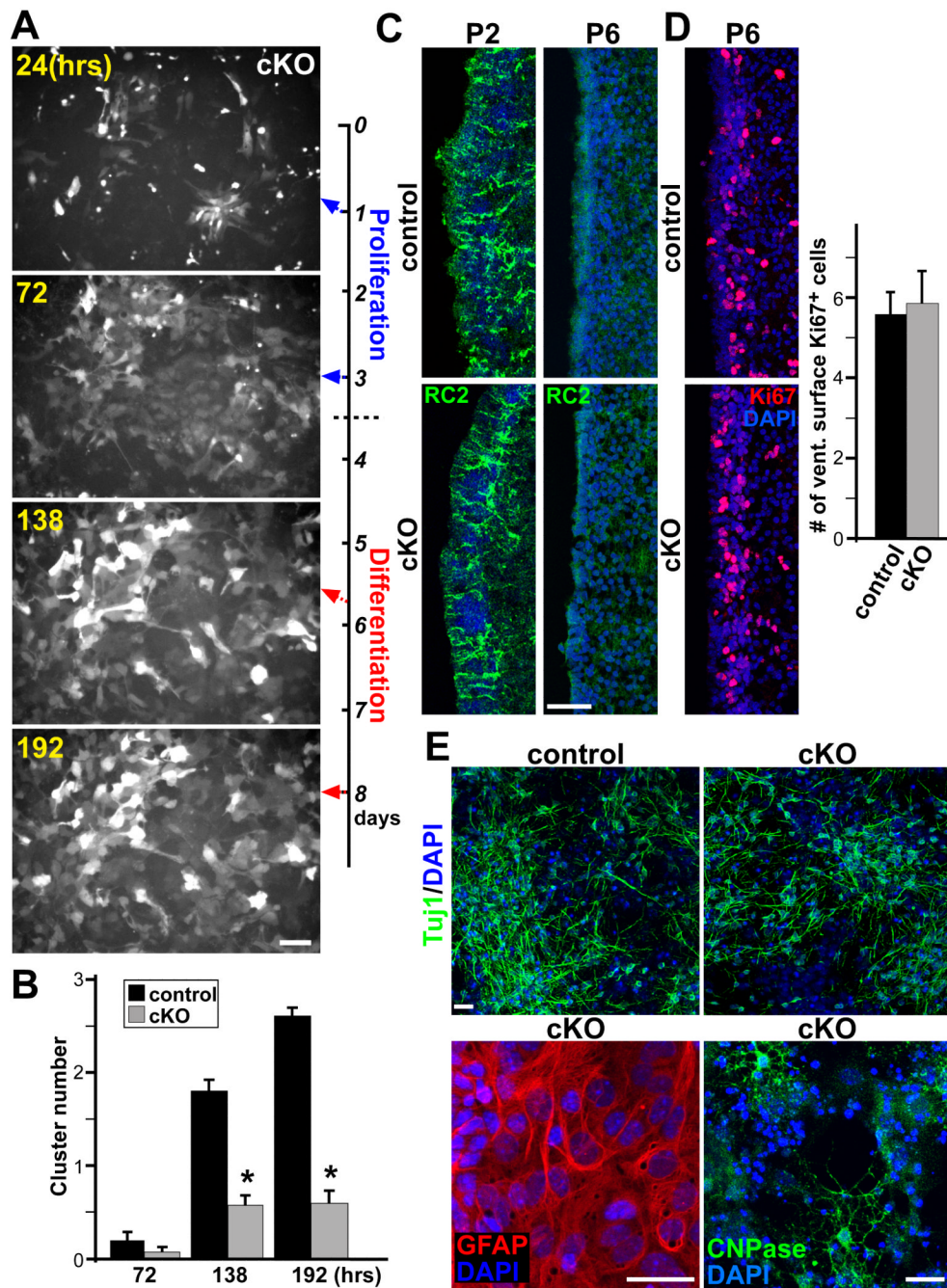
**Figure 6. Radial glial transition to SVZ stem cells in conditional Foxj1 mutant mice**
(A) Stills from time-lapse live imaging movies of Foxj1-GFP[+] cKO pRGPs during in vitro differentiation. Note the general lack of clustering between GFP-bright cells (also see Movie S3). (B) Quantification of cellular clustering from live imaging movies (see Figure S6A for details). * p < 0.05 Wilcoxon 2-sample test; error bar = sem; n = 5. (C) RC2 IHC staining of lateral ventricular wall sections, showing the presence (P2) and down-regulation (P6) of RC2 expression in both control and cKO mice. (D) IHC staining and quantification of Ki67^{+} cells on the ventricular wall surface from P6 control and cKO mice. n = 9. (E) In vitro differentiation of SVZ adherent neural stem cell cultures from P6 control and cKO mice,

showing production of Tuj1$^+$ neurons, GFAP$^+$ astrocytes, and CNPase$^+$ oligodendrocytes. Scale bar: (A, C, D) 50 μm; (E) 15 μm. See also Figure S7.
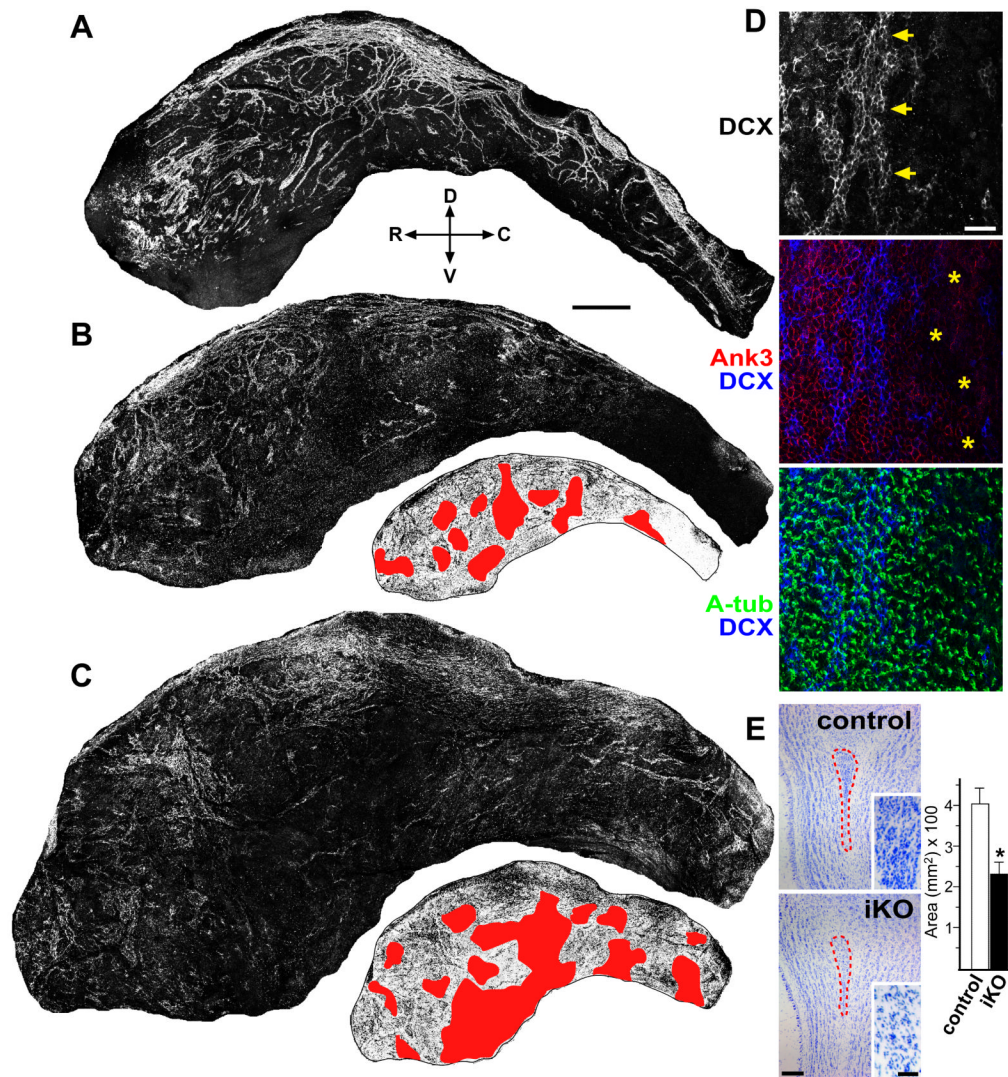
**Figure 7. Inducible SVZ niche disruption results in neuroblast chain defects**

IHC staining of ventricular wall wholemounts from P28 mice injected with tamoxifen at P14. (A) In control animal, DCX antibody staining showed the abundance of neuroblasts assembled into chains. R: rostral, C: caudal, D: dorsal; V: ventral. (B) *foxj1-CreER$^{t2}$; foxj1$^{KO/Flox}$* (iKO) mouse injected with tamoxifen showed disorganization in DCX$^+$ neuroblast chains. Corresponding inverted image are marked with red showing areas of substantial Ank3 disruption on the ventricular surface. (C) Another example from iKO animal with tamoxifen injection. Corresponding inverted image shows large patches of ventricular Ank3 disruption and ventricular enlargement. (D) Close-up Z-stack images of ventricular wholemount from iKO animal showing neuroblast chain boundary (arrows) and areas of missing Ank3 (asterisks). Acetylated-tubulin (A-tub) shows surface cilia. (E) Nissl staining of olfactory bulb sections from control and iKO mice, showing defects in size (dashed areas, quantified) and cell density (insets) within the RMS. * $p < 0.01$ Wilcoxon 2-sample test; error bar = stdev.; n = 5. Scale bar: (A-C) 500 μm; (D) 20 μm; (E) 200 μm / close-up 50 μm. See also Figure S8.
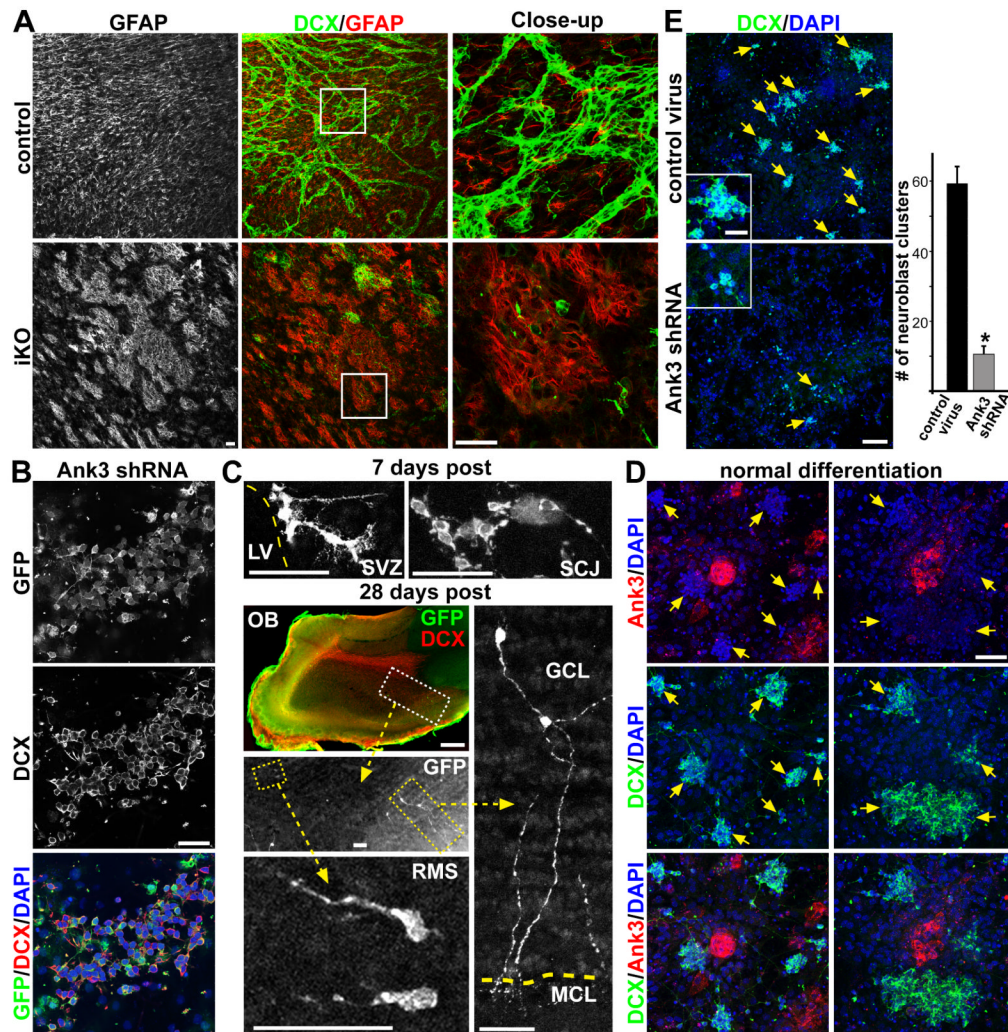
**Figure 8. Ank3 expression in SVZ niche is required for neuroblast production**
(A) IHC staining of ventricular wholemounts from P28 control and iKO mice injected with tamoxifen at P14, showing abnormal GFAP+ patches in targeted areas. (B) SVZ NSC adherent culture from wild-type mice infected with lentivirus expressing Ank3 shRNA and GFP driven by ubiquitous EF1α promoter, showing abundant GFP+DCX+ neuroblasts 4 days after in vitro differentiation. (C) GFP staining of brain sections from mice transplanted with Ank3 shRNA-infected SVZ NSC culture, 7 and 28 days post transplantation. SCJ = striatal cortical junction; RMS = rostral migratory stream; GCL = granular cell layer; MCL = mitral cell layer. (D) IHC staining of wild-type pRGP niche cultures: 5 days after plating large numbers of DCX+ neuroblast clusters can be seen as well as Ank3+ niche progenitor clusters. (E) pRGP niche cultures infected with control versus Ank3 shRNA lentivirus, showing a dramatic reduction in the numbers of DCX+ neuroblast clusters (arrows), and quantified below (each cluster has greater than 5 DCX+ cells per DAPI staining, using same software acquisition as described in Figure S4B). * p < 0.01 Wilcoxon 2-sample test; error bar = stdev.; n = 5. Scale bar: (A) 50 μm; (B) 25 μm; (C) OB 500 μm, all others 50 μm; (D) 50 μm; (E) 100 μm / close-up 25μm.